GRANT / AMES

33 pages

IN-28450

Toward Comparing Experiment and Theory for Corroborative Research on Hingeless Rotor Stability in Forward Flight

(An Experimental and Analytical Investigation of
Isolated Rotor-Flap-Lag Stability in Forward Flight)

Annual Report Under Grant No.NCC 2-361

By G. Gaonkar

Prepared for the Aeroflight Dynamics Directorate

U. S. Army Aviation Research and Technology Activity

Ames Research Centre

Moffett Field, CA 943035-1099

FLORIDA ATLANTIC UNIVERSITY
Department of Mechanical Engineering
School of Engineering
Boca Raton, FL 33431

August 1986

An Experimental and Analytical Investigation of Isolated Rotor Flap-Lag Stability in Forward Flight

ABSTRACT

For flap-lag stability of isolated rotors, experimental and analytical investigations are conducted in hover and forward flight on the adequacy of a linear quasisteady aerodynamics theory with dynamic inflow. Forward flight effects on lag regressing mode are emphasized. Accordingly, a soft inplane hingeless rotor with three blades is tested at advance ratios as high as 0.55 and at shaft angles as high as 20°. The 1.62-m model rotor is untrimmed with an essentially unrestricted tilt of the tip path plane. In combination with lag natural frequencies, collective pitch settings and flap-lag coupling parameters, the data base comprises nearly 1200 test points (damping and frequency) in forward flight and 200 test points in hover. By computerized symbolic manipulation, a linear analytical model is developed in substall to predict stability margins with mode indentification. To help explain the correlation between theory and data it also predicts substall and stall regions of the rotor disk from equilibrium values. The correlation shows both the strengths and weaknesses of the theory in substall.

NOMENCLATURE

a	Lift curve slope, rad^{-1}
c_d	Profile drag coefficient
N	Number of blades

R	Flap-lag structural coupling parameter
r	Dimensionless (1/R) radial position
t	Dimensionless time (identical with blade azimuth position of the first blade).
α	Angle of attack
α_s	Rotor shaft angle, positive nose down
μ	Advance ratio
β_o (ζ_o), β_s (ζ_s) and β_c(ζ_c)	Multiblade flapping (lag) coordinates: collective and first order cyclic flapping (lag) components
θ	Equilibrium pitch angle= $\theta_o+\theta_s\sin\psi_k+\theta_c\cos\psi_k$
$\bar{\lambda}$	Total inflow ratio = $\mu\tan\alpha_s+\bar{\nu}$
$\bar{\nu}$	Steady induced flow = $\bar{\nu}_o+\bar{\nu}_s\ r\ \sin\psi_k + \bar{\nu}_c\ r\ \cos\psi_k$

ν_o ($\bar{\nu}_o$), ν_s ($\bar{\nu}_s$) and ν_c(ν_c)	Uniform, side-to-side and fore-to-aft unsteady (steady) induced flow
Ω	Rotor rotational speed in rpm
ω_ζ	Dimensionless ($1/\Omega$) uncoupled lag frequency
ψ_k	Azimuth position of the k-th blade
γ	Lock number
$(\cdot)$	d/dt
$\lvert\ \rvert$	absolute value

1. INTRODUCTION

Relatively few investigations with concomitant corroboration of test data have been conducted on isolated rotor instabilities.[1-3] Such an investigation is particularly desirable for inplane modes which are at best weakly damped and for which the state-of-the art of predicting damping levels merits considerable refinements.[4-8] Here, we study some basic aspects of that investigation concerning the flap-lag stability of a three-bladed rotor in hover and forward flight ($0 \leq \mu \leq .55$). An experimental model is used with intentionally built-in structural simplicity to facilitate isolate the ingredients that participate in the correlation. The analytical model is based on quasisteady aerodynamics with dynamic inflow and it is directly tailored to fit the experimental model. The correlation refers to the lag regressing mode [9] which is independent of the number of blades per se.[4, 10, 11] Further, compared to other modes, it is the lowest-frequency mode and is better suited to assessing the validity of the quasisteady aerodynamics theory. Although the theory merits substantial refinements in stall ($\alpha > |12^\circ|$), we have included some correlation in stall as well. Such inclusion provides an improved interpretation of the correlation

between measured and predicted data.

A specific rotor is investigated under untrim conditions[4,11] ($\theta_s=\theta_c=0$), cyclic flapping present) and the prediction is based on a linear theory. However, from an intentionally simplified experimental model, the correlation makes use of a comprehensive data-base of nearly 1400 test points with respect to Ω, R, θ_o, α_s and μ. Such a correlation should give generally applicable qualitative results on the adequacy of the linear theory when stall is not an issue and should promote further refinements.

2. EXPERIMENTAL MODEL

The model tested was a three-bladed hingeless rotor with a diameter of 1.62 m. The rotor was designed to closely approach the simple theoretical concept of a hingeless rotor as a set of rigid, articulated blades with spring restraint and coincident flap and lead-lag hinges. This was accomplished by the "folded back" flexure design shown in an exploded view in Fig. 1. Taking the center of the flexural elements as the effective hinge point gives a non-dimensional hinge offset of 0.11 for the design. The blades were designed to be very stiff relative to the flexures so that the first flap and lead-lag modes involve only rigid body blade motion. The influence of the torsional degree of freedom was minimized by keeping the first torsion frequency as high as possible. In particular, the first torsion mode frequency was above 150 Hz non-rotating, insuring a rotating first torsion frequency of at least 9/rev over the entire rotor speed range tested. The rotor properties are summarized in Table 1.

The rotor had no cyclic pitch control, and collective pitch was set manually. The blade pitch could be set by changing the angle of the blade relative to the flexure at the blade-flexure attachment, giving a structural coupling value of zero, or by changing the angle of the entire blade-flexure assembly relative to the hub, giving a structural coupling value of one.

The test stand on which the rotor was mounted included a roll gimbal which could be locked out mechanically. Rotor excitation was accomplished through this gimbal by a 50 lb (11.2N) electromagnetic shaker. The stand was designed to be as stiff as possible so that the test would closely represent the case of an isolated rotor. However, the lowest frequency of the installed stand with the gimbal locked and the rotor mounted was found to be 31 Hz, somewhat lower than what was desired. The entire test stand could be pitched forward with an electric actuator to control the rotor shaft angle. The shaft angle provided the only means of controlling the rotor loads at a given collective pitch and advance ratio. A photograph of the model installed in the wind tunnel is shown in Fig. 2.

3. ANALYTICAL MODEL

The analytical model consists of an offset-hinged rigid lag-flap model with flap and lag spring restraints at the offset hinge. The spring stiffnesses of the math model are selected such that the uncoupled rotating flap and lag natural frequencies coincide with the corresponding first-mode non-rotating natural frequencies of the elastic blade. The effect of the hinge offset, which is 11.1% in lag and flap, is accounted for in rotor trim and stability analyses. The rotor is untrimmed, with an essentially unrestricted tilt of the tip path plane.[4, 11] The rotor angular velocity is Ω, and with time unit $1/\Omega$, the azimuth angle of the first or the reference blade represents the dimensionless time t. The distribution of flexibility between the hub including flexures and the blade (outboard of the blade location where pitch change takes place) is simulated by an elastic coupling parameter R which is also referred to as the hub rigidity parameter. Basically, R relates the rotation of the principal axes of the blade-hub system and the blade pitch θ.

The blade airfoil aerodynamics is based on linear, quasisteady theory in

substall (angle of attack $\alpha<|12°|$) without inclusion of compressibility or other effects due to reversed and radial flow. Steady non-uniform inflow with first harmonic distribution ($\bar{\nu} = \bar{\nu}_o + \bar{\nu}_s r \cos\psi_k + \bar{\nu}_c r \sin\psi_k$)is assumed. The airfoil nonlinear section effects are neglected.[7,8] For the math model we take a=5.73 and c_d = 0.0079 (NACA 23012). [7,8] The dynamic inflow effects are included from a 3x3 inflow model based on an unsteady actuator-disk theory---the Pitt Model, which has been recently verified experimentally. [5] The equations of motion including the multiblade coordinate transformation are derived from symbolic manipulation [12,13]. For the three-bladed rotor, the 15x1 state vector comprises 12 multiblade components (β_o, $\dot{\beta}_o$, β_s, $\dot{\beta}_s$, β_c, $\dot{\beta}_c$, ζ_o, $\dot{\zeta}_o$, ζ_s, $\dot{\zeta}_s$, ζ_c, $\dot{\zeta}_c$) and 3 dynamic inflow components (ν_o, ν_s, ν_c). The computational details of Floquet transition matrix, and of damping levels and Floquet eigenvectors are respectively as in references 14 and 13.

4. EXPERIMENTAL PROCEDURES

An experimental investigation of the rotor's lead-lag stability characteristics in hover and, especially, forward flight was conducted in the Aeroflight Dynamics Directorate's 7-by-10 foot (2.1-by-3.0 m) wind tunnel. The data was collected in two tunnel entries, the first in the summer of 1982 and the second in the summer of 1983. The model's configuration and the test procedures used were the same for both tests. The only exception to this is that for the 1982 test the hover data was taken with the wind-tunnel test section doors open and the windows removed in an attempt to reduce recirculation effects. In 1983 the hover data were taken incidental to forward flight data (Ω=750 and 1000 rpms) so the windows were left in place and doors were closed. The rotor plane itself was located about 0.63 rotor diameters above the test section floor (with the shaft vertical). However the influence of recirculation

and ground effect on the hover data are not significant. [15]

For each data point obtained, the blade pitch was set manually and the rotor was tracked. The rotor was then brought up to speed and wind tunnel dynamic pressure was increased to obtain the desired advance ratio while adjusting the shaft angle to keep the rotor flapping loads within limits. Once at the test condition, the roll gimbal was unlocked and the shaker was used to excite the model at the appropriate frequency. When a good level of excitation was evident in the output of the lead-lag bending gages, the shaker was cutoff, the roll gimbal locked out, and then transient data acquisition commenced. The data itself was digitized on-line with a sample rate of 100 Hz and a total record length of 5.12 seconds. The data was then transformed to the fixed system coordinates. Spectral analysis and the moving block technique[16] were used to determine the frequency and damping of the response. At least two data points were obtained at each test condition and the scatter between the measurements was found to be very small.

Progressing and regressing lead-lag mode data were obtained for the hover test conditions, but above about 600rpm the progressing mode was found to be contaminated by coupling with the lower stand mode. Because all of the forward flight conditions tested were above this rotor speed, no progressing mode data were obtained. The regressing mode data should be representative of isolated blade results over the entire rotor speed range tested and appears to be of very good quality. The hover test envelopes for both the 1982 and 1983 tests are shown in Fig. 3(a) and the forward flight test envelopes are shown in Fig. 3(b). The edges of the forward flight envelopes were set by the maximum allowable rotor flapping loads.

Table 1: Measured Model Properties

Number of Blades	3
Radius	0.81 m
Chord	0.0419 m
Airfoil Section	NACA 23012
Non-dimensional Hinge Offset	0.111
Blade Inertia About Hinge	0.01695 kg-m^2
Blade Mass Center Distance from Hinge	0.188m
Blade Mass (Outboard of Hinge)	0.204 kg
Non-rotating Flap Frequency	3.09 Hz
Non-rotating Lead-lag Frequency	7.02 Hz
Average Lead-Lag Structural Damping Ratio	0.19% critical
Lock Number γ (based on a=5.73)	7.54

5. CORRELATION OF THEORY AND DATA

We, now come to presenting the correlation between the measured and predicted data in hover and forward flight ($0 \leq \mu \leq 0.55$). If not stated otherwise, the predicted values based on a linear theory include dynamic inflow and uniform steady inflow and the measured values include both the 1982 and 1983 test points (figure 3). To facilitate an appreciation of the scope of the correlation, we begin with an overview of the data-base. As seen from figure 3, the hovering and forward flight cases refer to zero and full structural coupling (R=0 and 1)in combination with varying rotational speeds in hover ($0 \leq \Omega \leq 1000$ rpm) and with two rotational speeds (Ω=750 and 1000 rpms) in forward flight. Further, we have four values of collectives in hover(θ_o= 0°, 4°, 6° and 8°) and three values of collectives in forward flight (θ_o = 0°, 3° and 6°). Compared to hover,

the data in forward flight is much broader in scope, since for each collective, the shaft tilt varies from 0° to 20° in combination with different advance ratios as shown in figure 3b. Thus, given the extensive scope of the data base and the corresponding predicted values, only a small portion of the total correlation is presented for the damping levels. (Frequency-data correlation is available in reference 17.) We also emphasize how far we can isolate different ingredients that participate in the correlation. In particular, those ingredients refer to nonuniform steady inflow and unsteady or dynamic inflow. In several cases, we also refer to nonlinear drag in substall ($|\alpha| \leq 12°$) and to stall ($|\alpha| > 12°$), and heuristically identify the deviation between the theory and data with the non-linear airfoil characteristics. However, it is good to reiterate the following. The nonlinear airfoil section properties including those of drag in substall are not included. Though a linear theory is used, we include correlation even when an appreciable portion of the rotor disk ($\geq$ 10%) is in stall. That inclusion together with stall region contours provides a better understanding of the adequacy of the linear theory and also of the role of airfoil aerodynamic nonlinearity.

With this as a background, we take up figure 4 which shows the lag regressing mode damping versus the rotor rotational speed for four values of collectives, $\theta = 0°$, 4°, 6° and 8°. For zero pitch setting, the angle of attack is very low. This fact is well reflected in the excellent correlation between theory and data except for minor discrepancies for very low rotational speeds (say, $\Omega < 300$ rpm). Those discrepancies are consistently observed for all the four cases of collectives for $\Omega < 300$ rpm, when the predicted damping level is less than the data. The reasons for this are not known. Also for $\theta_o = 4°$, 6° and 8°, the correlations is generally good. However, for $\Omega > 800$ rpm, the theory deviates from the data and that deviation increases with increasing blade pitch (compare the case for $\theta_o = 4°$ with that for $\theta_o = 8°$). The 1.62-m model

was tested in a 2.13 x 3.05 meter test section and the ratio of model height to rotor diameter was only 0.63, a relatively low value. Therefore, additional damping values were predicted with empirical corrections for ground and recirculation effects (that is, replacing $\bar{\nu}$ by $k\bar{\nu}$, where $k<1$ for ground effect and $k>1$ for recirculation). It was found that those deviations between theory and data are not associated with ground and recirculation effects. Though our approach to capture those effects is empirical, recent experimental evidence supports this finding. [15] Though the data are within substall ($|\alpha| \leq 12°$), the Reynolds number is very low ($\approx$17000). Nonlinear airfoil drag characteristics are generally associated with such deviations [1,7,8] and they are currently being investigated. Thus, in summary, figure 4 shows that the data are in general agreement with the theory.

Coming to the forward flight case, we start with the damping data for the zero-collective case with Ω = 1000 rpm and R = 0, figures 5 and 6. Figure 5 shows the damping data as a function of advance ratio for discrete values of shaft tilt α_s. Figure 6 is a cross plot of the data in Figure 5, that is, damping as a function of α_s for discrete values of advance ratio μ. Thus, figure 5 together with figure 6 provides an improved picture of the correlation between theory and data for increasing values of shaft tilt α_s and advance ratio μ. Overall, figures 5 and 6 show good correlation and exhibit two main features. First, compared to the correlation for high values of $\mu\alpha_s$, the correlation is much better for low values of $\mu\alpha_s$. For example, at low advance ratios (μ=0.1 and 0.2), the correlation is remarkable even quantitatively, virtually for the entire range of shaft tilt ($0 \leq \alpha_s \leq 20°$). So is the case the for low values of shaft tilt ($\alpha_s \geq 4°$) and for advance ratios as high as 0.55, see figure 5 for α_s = 4°. For the high advance ratio case of 0.3, the correlation is equally remarkable for $\alpha_s \leq 8°$. For μ=0.4 and $\alpha_s \leq 4°$ (figure 6), the theory slightly underpredicts damping. Nevertheless, the correlation is satisfactory

and the reasons for these minor discrepancies of underprediction are not known. That the theory shows remarkable agreement with the data for low values of $\mu\alpha_s$ is to be expected. After all, the pitch setting is zero and therefore the angle of attack is very low for low values of $\mu\alpha_s$. Coming to the second feature, we observe that with increasing μ and α_s, the theory consistently overpredicts damping and increasingly deviates from the data. For example see figure 6 for μ=0.3 and $\alpha_s>10°$ and for μ=0.4 and $\alpha_s>6°$. This is also to be expected, because the angle of attack is found to increase rapidly with increasing values of $\mu\tan\alpha_s$. However, except for $\alpha_s>14°$ at μ=0.4 (figure 6) prediction is qualitatively accurate at high advance ratios (μ=0.3 and μ=0.4) in that the theory predicts the correct trend of increasing damping with increasing α_s, as does the data. For μ=0.4 and $\alpha_s\geq14°$, the qualitative accuracy is not that evident and merits additional comments. As seen from the data envelope from figure 3b for θ_o=0° and μ=0.4, the data point for $\alpha_s\geq12°$ are limited. Nevertheless, the data points at α_s=12°, 14° and 16° in figure 6 do show that the damping level more or les levels off for $\alpha_s>12°$. In any case, for μ=0.4 and $\alpha_s>12°$,the predicted trend of damping which increases consistently and appreciably with respect to α_s, is not exhibited by the data.

The preceding correlation for zero pitch setting shows that the discrepancy between theory and data increase with increasing values of $\mu\tan\alpha_s$. To facilitate explain this discrepancy, we refer to the stall regions of the rotor disk based on equilibrium values and use the percent stall area of the rotor disk as an objective measure of the stall effects on the theory. Figures 7a and 7b show two typical stall region ($|\alpha|<12°$) contours for μ=0.3 and 0.5. We also observe in passing that for μ=0.2 and $\alpha_s\leq20°$, the stall region (not shown) hardly exceeds 6% of the rotor disk.[17] This observation corroborates the fact that the theory exhibited excellent agreement with the data for μ=0.1 and 0.2 in figure 6. As seen from figures 7a and 7b nearly 20% of the rotor disk is in

stall for μ=0.3 and α_s=16° and for μ=0.5 and α_s=8°. It is also seen that slightly more than 10% of the rotor disk is in stall for μ=0.3 and α_s=12° (figure 7a), for μ=0.4 and α_s=6° (reference 17) and for μ=0.5 and α_s=4° (figure 7b). Since the blade has zero pitch setting, the area of the stall region increases rapidly with increasing values of μ and α_s, and at the low test Reynolds number (≈170,000) the effects of airfoil aerodynamic nonlinearity become more pronounced. Therefore, with increasing values of μ and α_s, those effects seem to mask the predicted data increasingly and account for the increasing deviation between theory and data. A similar situation exists for the second set of data for 3° collective, taken up next.

While figure 8 refers to zero flap-lag coupling with Ω=1000 rpm, figure 9 refers to full flap-lag coupling with Ω=750 rpm. Both figures essentialy show the same feature. That is, the correlation is qualitatively accurate only for low values of μ and α_s. By comparison, the correlation becomes qualitatively inaccurate with increasing values of μ and α_s, the data showing decreasing damping and the theory predicting the opposite trend of increasing damping. To fill in details, we consider figure 8. For μ=0.2, even for α_s = 20°, the stall contour results (not shown) show that not more than 6% of the rotor disk experiences stall.[17] Thus, stall is not an issue for $\mu \leq 0.2$. However, it is seen that there is consistent difference between the theory and data. For example at μ=0.05 in figure 8, the theory under predicts damping for all values of α_s. This is possibly due to nonlinear drag in substall at the low test Reynolds number and the investigation is continuing. Figures 7c and 7d also show that an appreciable portion of the rotor disk experiences stall. For example, for μ=0.3 and α_s=14°, nearly 10% of the rotor disk is in stall and the stall region for μ=0.4 rapidly increases for $\alpha_s > 8°$. Thus in summary, nonlinear drag effects in substall and stall effects seem to be contributing to the discrepancies between theory and data in figures 8 and 9.

With figure 10 and 11, we come to the data-base for $\theta_\circ = 6°$ and $\mu < 0.2$, also see figure 3b. The data are limited to low advance ratios and stall is not an issue here. For the complete range of shaft tilt ($0 \leq \alpha_s \leq 20$), the data are available only for $\mu = 0.05$. The corresponding correlation is given in figures 11a (R=0) and 11b (R=1). It is seen that the overall prediction is not satisfactory. In fact, for $\alpha_s=20°$ ($0\leq\mu\leq0.15$)the prediction shows qualitatively incorrect trend of increasing damping with increasing μ, a trend that is not supported by the data. This feature is quite similar to the one referred to earlier in figures 8 and 9 for $\alpha_s>8°$. Given the appreciable deviations between the theory and data for the hovering case with comparable pitch setting at Ω=1000 (e.g. figure 4 at $\theta°=6°$), the deviations in figures 10 and 11 for μ=0.05 are not unexpected. Inspite of the appreciable underprediction, the data supports the theory in showing that the damping level virtually remains constant for the entire range of shaft tilt at μ=0.05.The present theory refined to include nonlinear drag effect in substall should provide a means of isolating that effect and a better understanding of the correlation in figures 10 and 11.

We mentioned earlier that the preceding prediction includes uniform steady inflow and dynamic inflow. The final set of correlation as presented in figures 11, 12 and 13, is used to isolate the effects of nonuniform steady inflow and dynamic inflow. In figure 11, the predictions from the linear theory are shown by full lines. The predictions from that theory refined to include nonuniform steady inflow and the predictions from that theory without dynamic inflow are respectively shown by broken lines with dots and by broken lines. It is seen that nonuniform steady inflow hardly influences correlation. By comparison, dynamic inflow improves correlation throughout, but not significantly. Compared to the case with R = 1, when the improvement is at best marginal, the improvement is much better for the case with R = 0. Though the correlation in figure 11 refers to one case of very low advance ratio, it is generally seen

that nonuniform steady inflow ceases to be an issue in improving the correlation. As for dynamic inflow, we further explore its effects in figure 12 for the hovering case, and in figure 13 for the forward flight case at high advance ratios of 0.3 and 0.45. Figure 12 is a partial reproduction of figure 4 for θ_o = 6° and 8°. However, for simplicity, only the average values of data are shown. The improvement due to including dynamic inflow is noteworthy. However, for Ω>800 rpm, the increasing discrepancy between theory and data, particularly with increasing pitch setting, remains virtually unaffected, even with inclusion of dynamic inflow. The correlations in figures 11 and 12 do demonstrate that it is highly desirable to include dynamic inflow in predicting implane damping. The correlation in figure 13 based on the 1982 data is extremely interesting. Here we have θ_o=0°, Ω=1000 rpm and R=0 at high advance ratios of 0.3 and 0.45. As seen from figures 7a and 7b, we should expect appreciable stall effects for α_s>10° at μ=0.30, and for α_s>4° at μ=0.45, to render the theory is suspect. Two features are worth mentioning. First, in substall the improvement due to dynamic inflow is negligible for μ=0.3. For μ=0.45 and α_s<4°, when the linear theory is reasonably valid, the differences in the predicted values without and with dynamic inflow are too small. Nevertheless dynamic inflow slightly degrades correlation. Second, the predicted data (without inflow), which also does not account for stall shows "better correlation" for the entire range of shaft tilt. However, stall effects increase with increasing values of μ and α_s and mask the prediction without and with dynamic inflow. The prediction in figure 13 needs to be resolved for the effects of airfoil aerodynamic nonlinearity at the low test Reynolds number for a valid treatment of isolating dynamic inflow effects.

6. CONCLUDING REMARKS

Thus far, we presented the correlation between theory and data on the lag regressing mode damping levels. That correlation leads to the following remarks:

1. In hover, the predictions are in general agreement with the data. However, some discrepancies at high rotational speeds and blade pitch settings are identified. It is suggested that those discrepancies, though in substall, are associated with the nonlinear airfoil drag characteristics at the low test Reynolds number.

2. In forward flight at θ_o=0° and 3°, the correlation is good when not more than 10% of the rotor disk is in stall. Minor discrepancies are perhaps associated with nonlinear drag effects. When an appreciable portion of the rotor disk is in stall (≈ 10% or more), the theory is at best qualitatively accurate for θ_o=0°, in that the theory and data show the same trend of increasing damping with increasing α_s and μ, though there is appreciable quantitative discrepancy. And for θ_o=3°, the theory and data respectively show the opposite trends of increasing and decreasing damping levels with increasing α_s and μ.

3. In forward flight at θ_o=6°, the data are limited to low advance ratios (μ <0.20) and the theory significantly deviates from the data. In fact, for α_s=20, the prediction shows appreciably increasing damping with increasing μ, whereas the data shows slowly decreasing damping with increasing μ. For μ=0.05, the data confirm the prediction that the damping level essentially remains constant for the entire range of shaft tilt ($0 \leq \alpha_s \leq 20°$), and the discrepancies betwen the data and prediction are of the same order of magnitude as those in hover for θ_o=6°. Stall is not a major issue here. As conjunctured for the hovering case, here also nonlinear airfoil drag characteristics may be affecting the predictions.

4. Effects of nonuniform steady inflow hardly affect the predictions.

5. The inclusion of dynamic inflow consistently improves correlation in hover and forward flight. However, at high advance ratios, cases are identified for which predictions without and with dynamic inflow are masked by the effects of aiarfoil aerodynamic nonlinearity to pass a judgement on dynamic inflow effects.

7. ACKNOWLEGEMENT

We are grateful to Messers. Robert Ormiston and William Bousman for their encouragement and extensive comments. We also thank Mrs. Antonia Margetis and Mrs. Nancy Ward Anderson for their hard work and persistence in word processing this paper. This work is sponsored by the U. S. Army Aeroflight Dynamics Directorate, NASA-Ames Research Center and administered under Grant NCC 2-361.

8. REFERENCES

1. Ormiston, R. A., " Investigations of Hingeless Rotor Stability", Vertica, Vol. 7, No. 2, 1983, pp. 143-181.

2. Friedmann, P. P., "Formulation and Solution of Rotary-Wing Aeroelastic Stability and Response Problems", Vertica, Vol. 7, No.2, pp.101-141, 1983.

3. Bousman, William G., "A Comparison of Theory and Experiment for Coupled Rotor-Body Stability of a Hingless Rotor" ITR Methodology Assessment Workshop, NASA Ames Research Center, Moffett Field, California, June 1983.

4. Nagabhushanam, J. and Gaonkar, G. H., "Rotorcraft Air Resonance in Forward Flight with Various Dynamic Inflow Models and Aeroelastic Couplings", Vertica, Vol.8, No. 4, December, 1984, pp. 373-394.

5. Gaonkar, G. H. and Peters, D. A., "A Review of Dynamic Inflow and Its Effect on Experimental Correlations" Proceedings of the Second Decennial Meeting on Rotorcraft Dynamics, AHS and NASA Ames Research Center, Moffett Field, California, November 7-9, 1984. Paper No. 13.

6. Neelakantan, G. R. and Gaonkar, G. H., "Feasibility of Simplifying Coupled Lag-Flap-Torsional Models For Rotor Blade Stability in Forward Flight", Vertica, Vol. 9, No.3, pp. 241 - 256.

7. Bousman, W. G., Sharpe, D. L., and Ormiston,, R. A., "An Experimental Study of Techniques for Increasing the Lead-Lag Damping of Soft Inplane Hingeless Rotors", Proceedings of the American Helicopter Society 32nd Annual National Forum, Washington, D. C., May 1976, Preprint No. 730.

8. Ormiston, R. A. and Bousman, W. G., "A Study of Stall-Induced Flap-Lag Instability of Hingeless Rotors", Preceedings of the American Helicopter Society 29th Annual National Forum, Washington, D. C., May 1973, Preprint No. 730.

9. Peters, D. A., and Gaonkar, G. H., "Theoretical Flap-Lag Damping with Various Dynamic Inflow Models," Journal of the American Helicopter Society, July 1980, Vol. 25, No. 3, pp.29-36.

10. Gaonkar, G. H. et al, "The Use of Actuator-Disc Dynamic Inflow for Helicopter Flap-Lag Stability", Journal of the American Helicopter Society, July 1983, Vol. 28, No. 3, pp 79-88.

11. Gaonkar, G. H., and Peters, D. A., "Use of Multiblade Coordinates for Helicopter Flap-Lag Stability with Dynamic Inflow," Journal of Aircraft, Vol. 17, No. 2, 1980, pp.112-118.

12. Nagabhushanam, J., Gaonkar, G. H., and Reddy, T.S.R., "Automatic Generation of Equations for Rotor-Body Systems with dynamic Inflow for A-Priori Ordering Schemes," Seventh European Rotorcraft Forum, Garmisch-Partenkirchen, Federal Republic of Germany, September 8-11, 1981, Paper No. 37

13. Nagabhushanam, J., Gaonkar, G. H., Srinivasan, P., and Reddy T.S.R., Users' Manual for Automatic Generation of Equations of Motion and Damping Levels for Some Problems of Rotorcraft Flight Dynamics, R & D Report, HAL-IISC Helicopter Program, Indian Institute of Science, Bangalore, India, October 1984.

14. Gaonkar, G. H., Simha Prasad, D. S., and Sastry, D. S. "On Computing Floquet Transition Matrices of Rotorcraft", Journal of the American Helicopter Society, Vol. 26, No. 3, July 1981, pp. 56-62.

15. Sharpe, D. L., An Experimental Investigation of the Flap-Lag-Torsion Aeroelastic Stability of a Small-Scale Hingeless Helicopter Rotor in Hover, AVSCOM-TR-89-A-9, January 1986.

16. Bousman, W.G., and Winkler, D.J. "Application of the Moving-Block Analysis" 22nd Structures, Structural Dynamics, and Materials Conference, Atlanta, Ga. April 1981. Paper 81-0653-CP.

17. Gaonkar, G. H., McNulty, M. J. and Nagabhushanam, J., "An Experimental and Analytical Investigation of Isolated Rotor Flap-Lag Stability in Forward Flight," Eleventh European Rotorcraft Forum, London, England, September 10-13, 1985, paper No. 66.

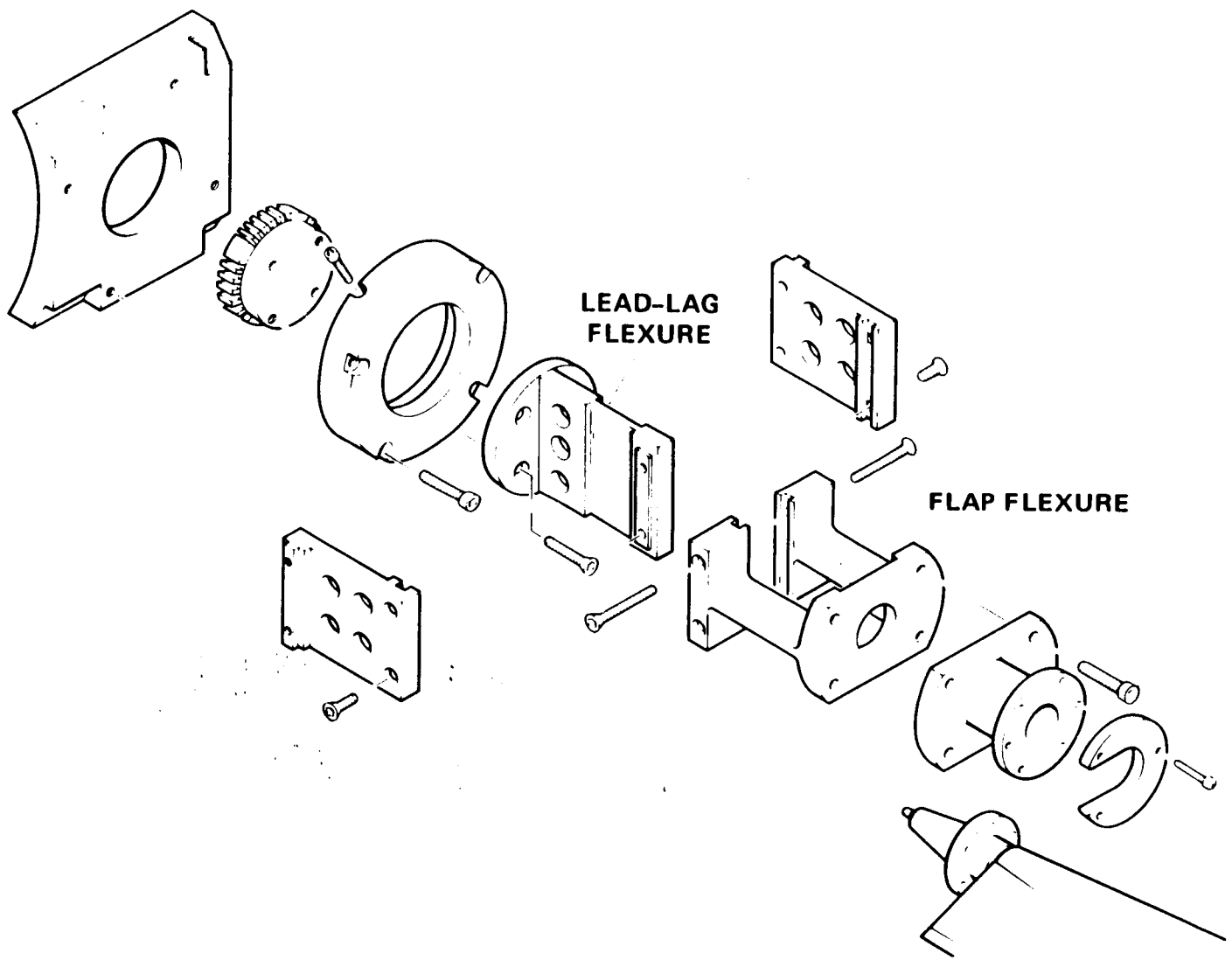

Figure 1. Exploded view of model flexure.

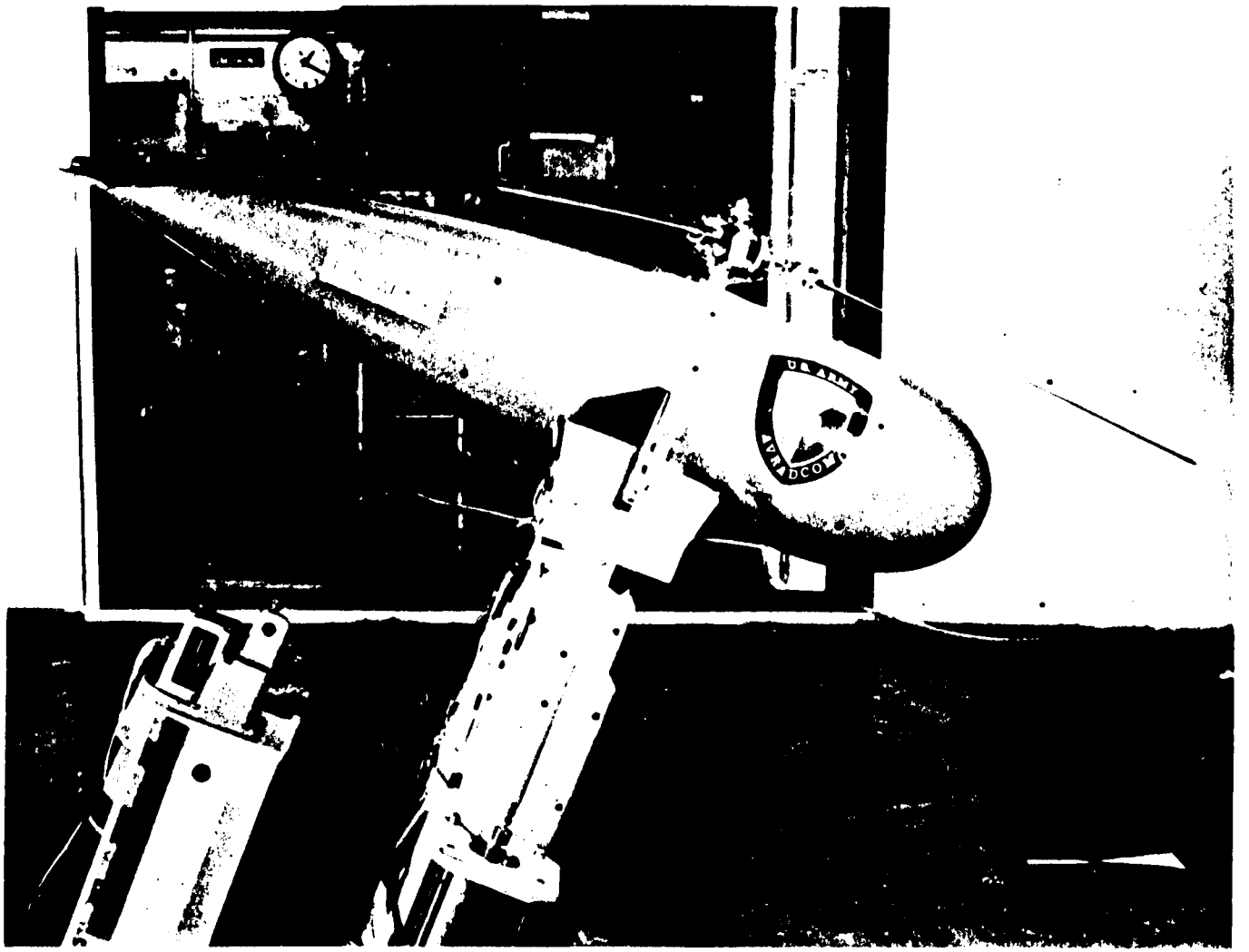

Figure 2. Model installed in the aeromechanics laboratory's 7-by-10-foot wind tunnel.

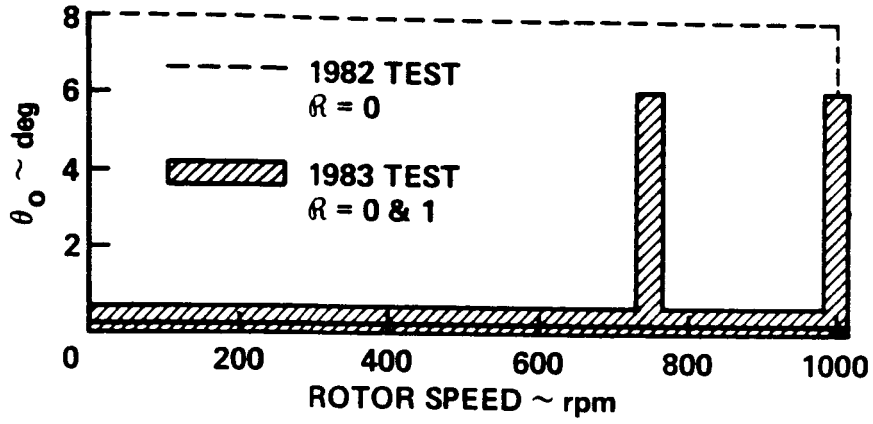

3(a) Hover tests.

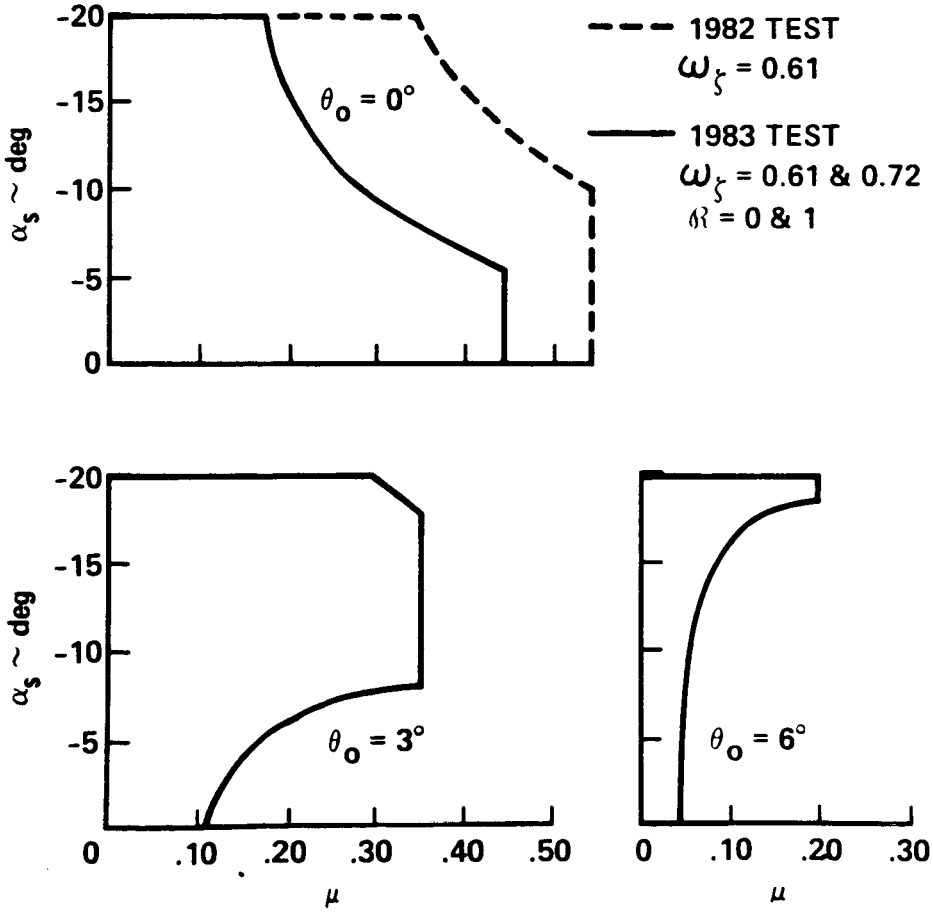

3(b) Forward flight tests.

Figure 3. Conditions tested.

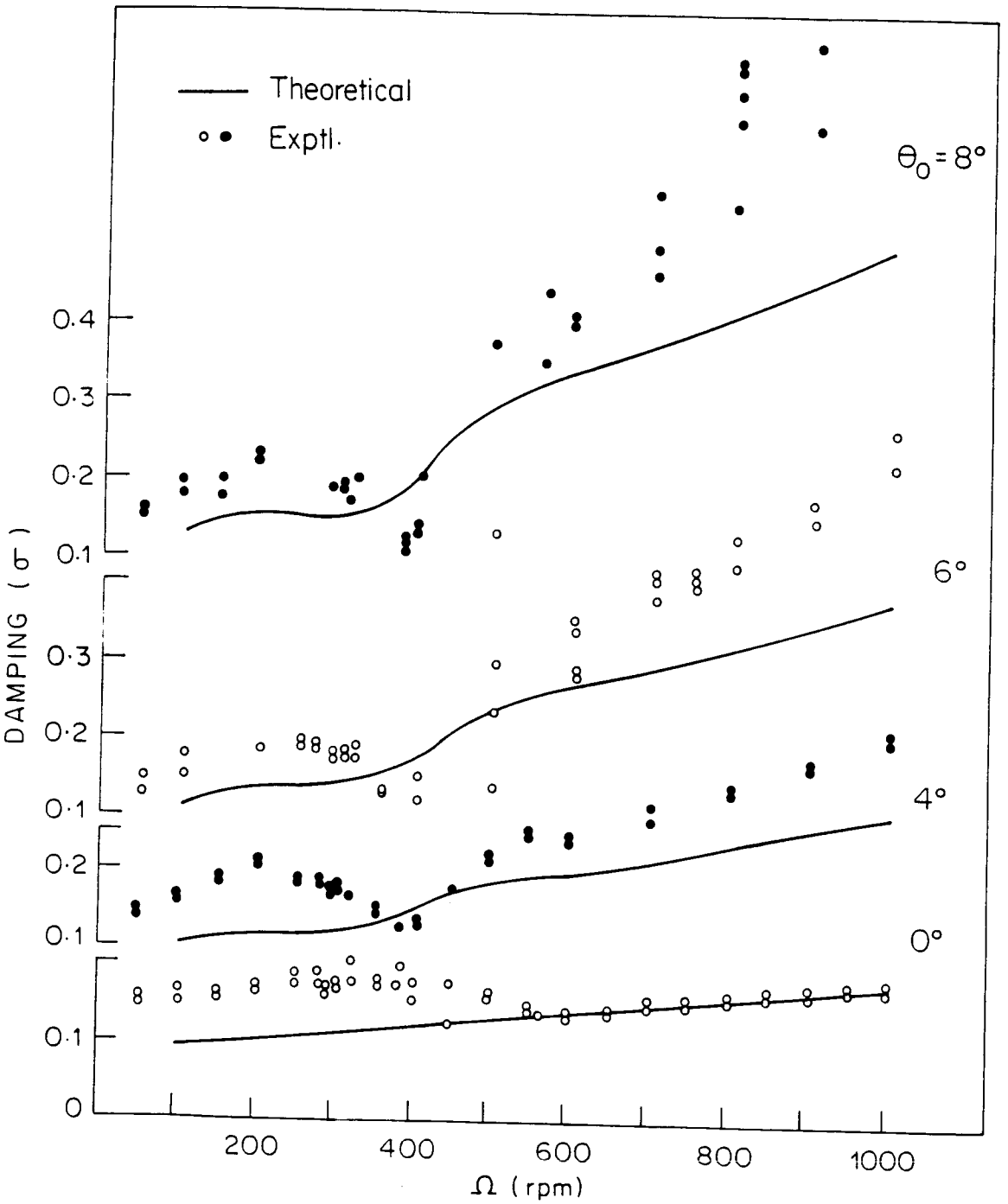

FIG. 4 LAG REGRESSING MODE DAMPING IN HOVER

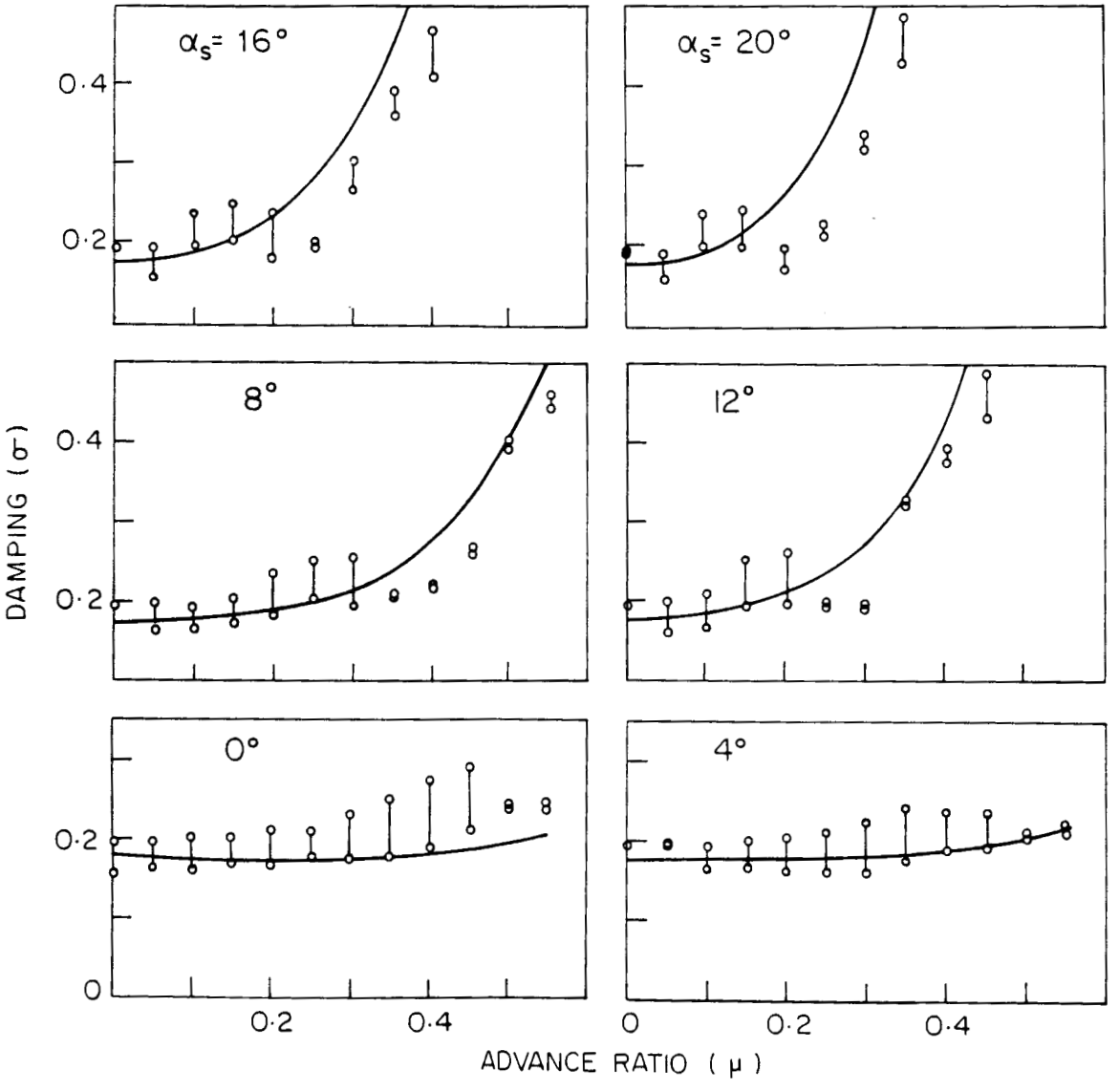

FIG. 5. LAG REGRESSING MODE DAMPING, θ_0= 0°, Ω = 1000, R = 0
(THEORETICAL ——, EXPTL. ∘∘)

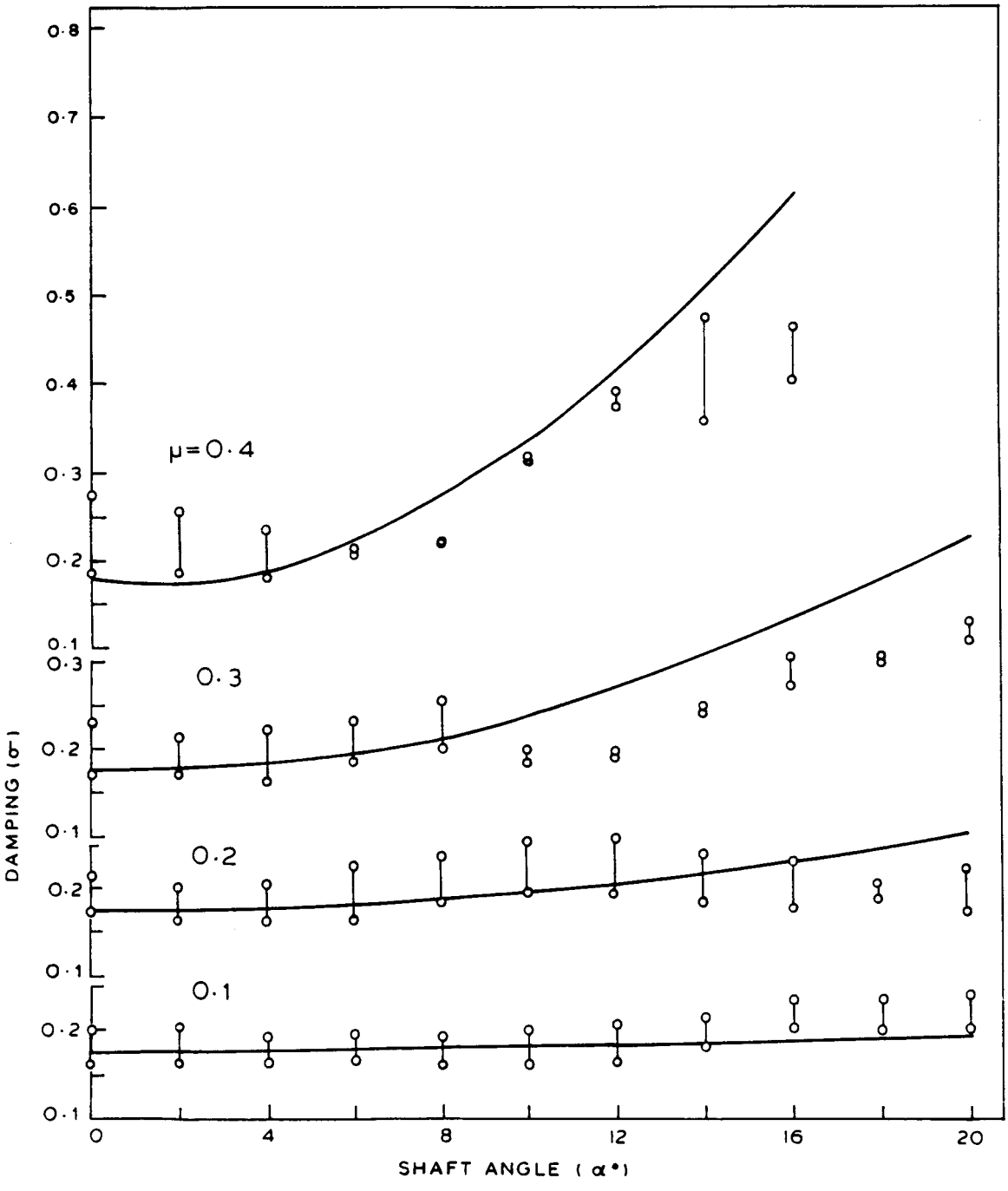

FIG. 6 LAG REGRESSING MODE DAMPING $\theta_0 = 0°$, $\Omega = 1000$ AND $R = 0$

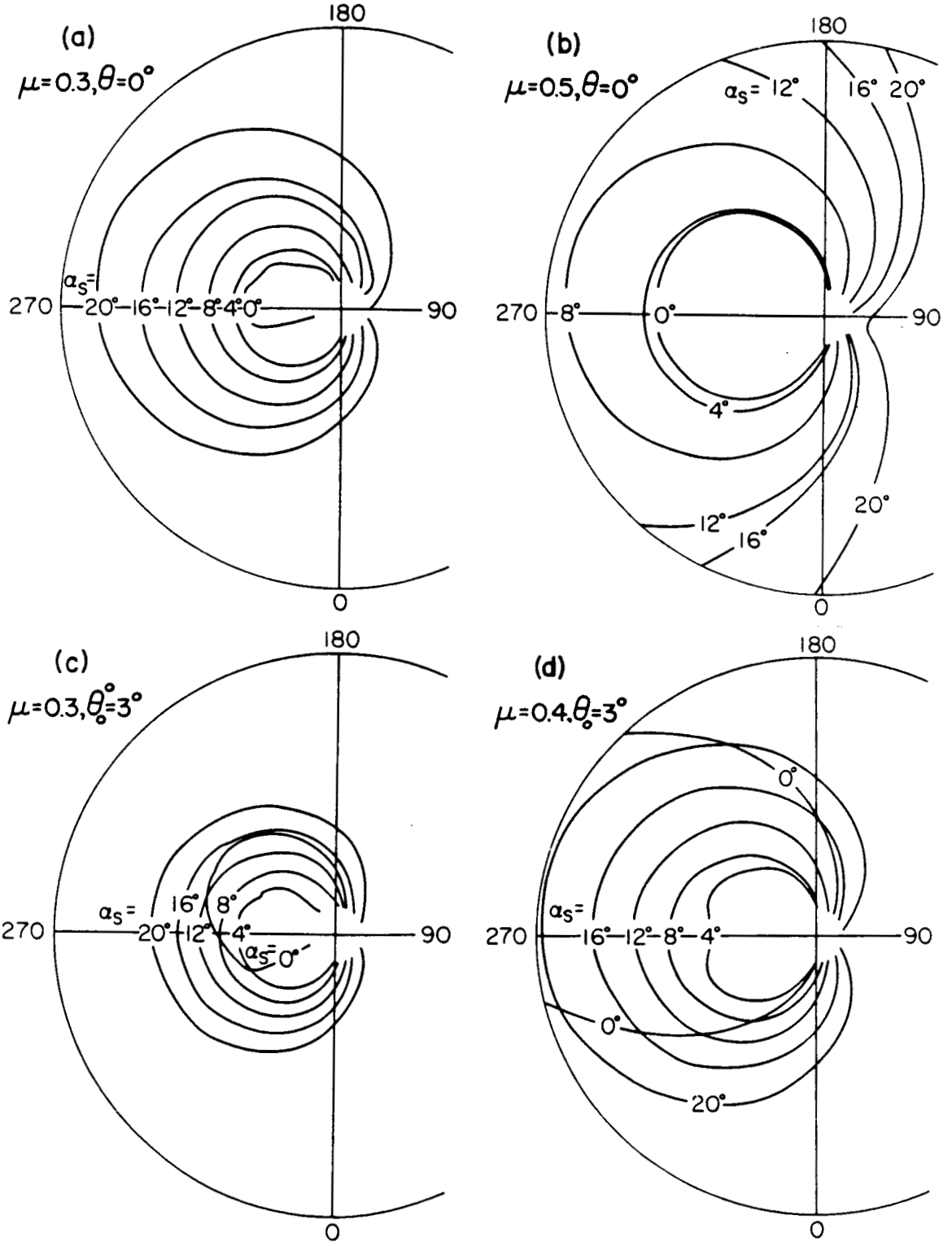

Fig. 7 STALL REGIONS, Ω=1000 RPM

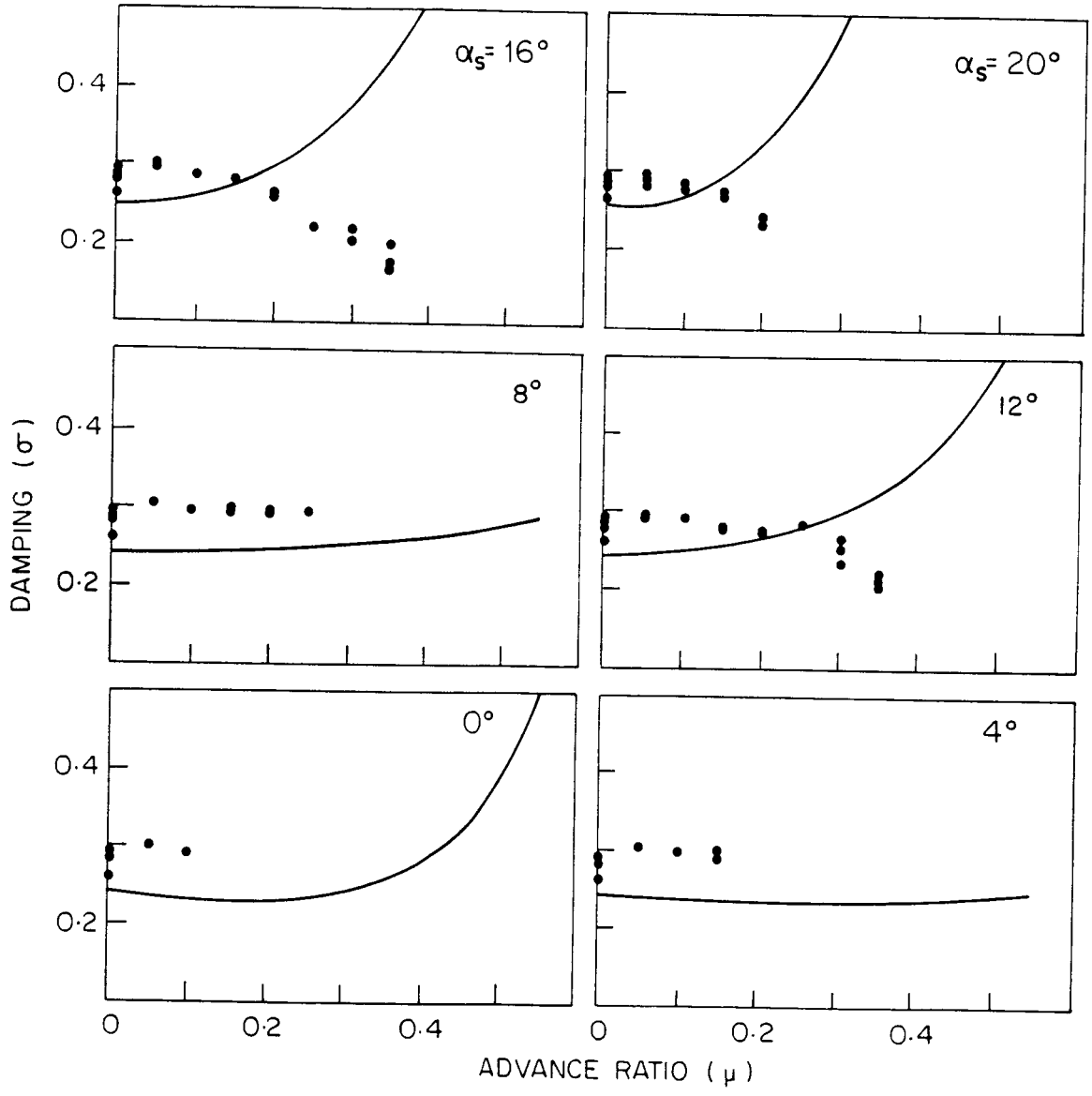

FIG. 8 LAG REGRESSING MODE DAMPING $\theta_0 = 3°$, R = 0, Ω = 1000
(THEORETICAL——, EXPTL. ••)

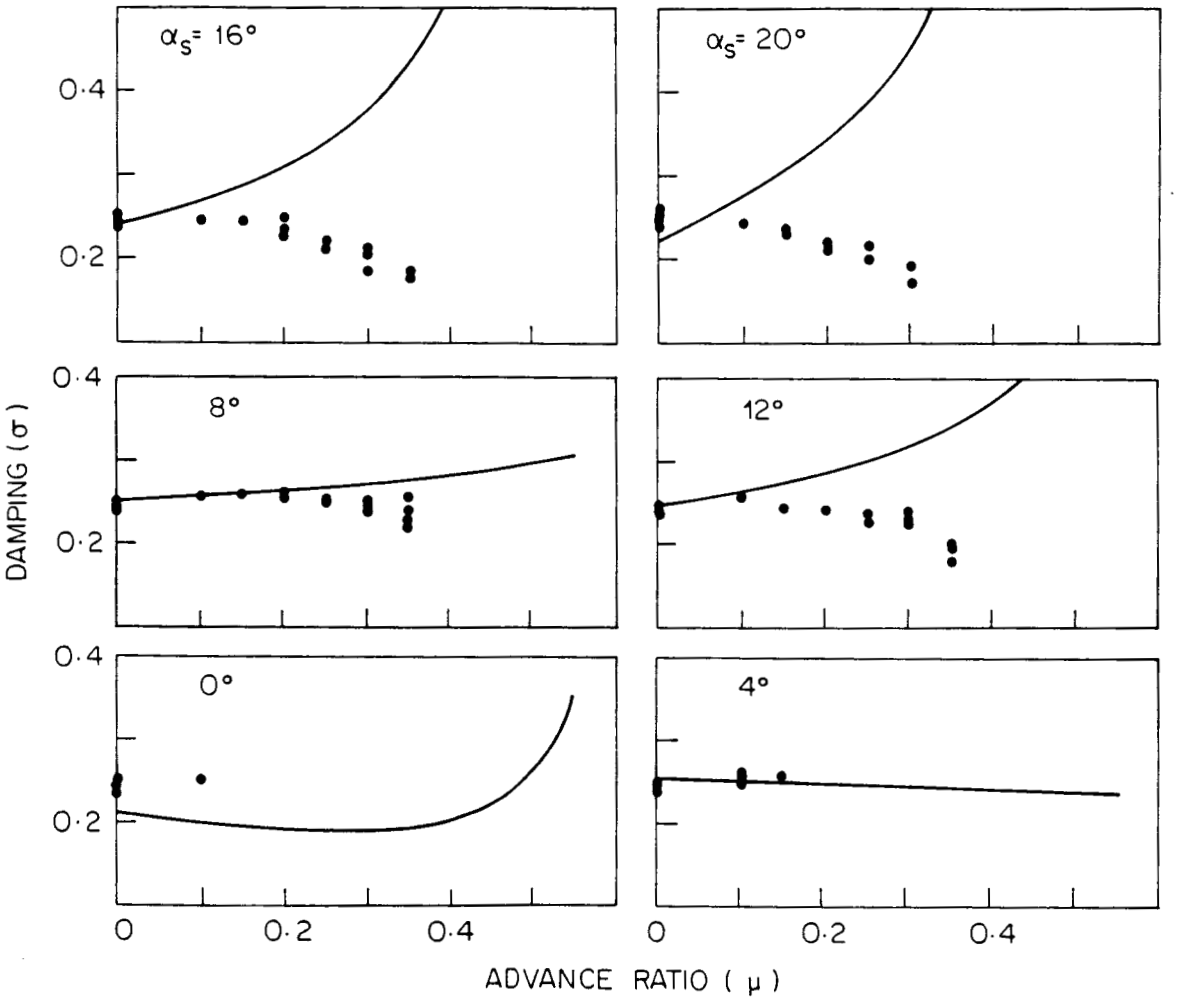

FIG. 9 LAG REGRESSING MODE DAMPING $\theta_0 = 3°$, $\Omega = 750$, $R = 1$
(THEORETICAL ——— , EXPERIMENTAL ••)

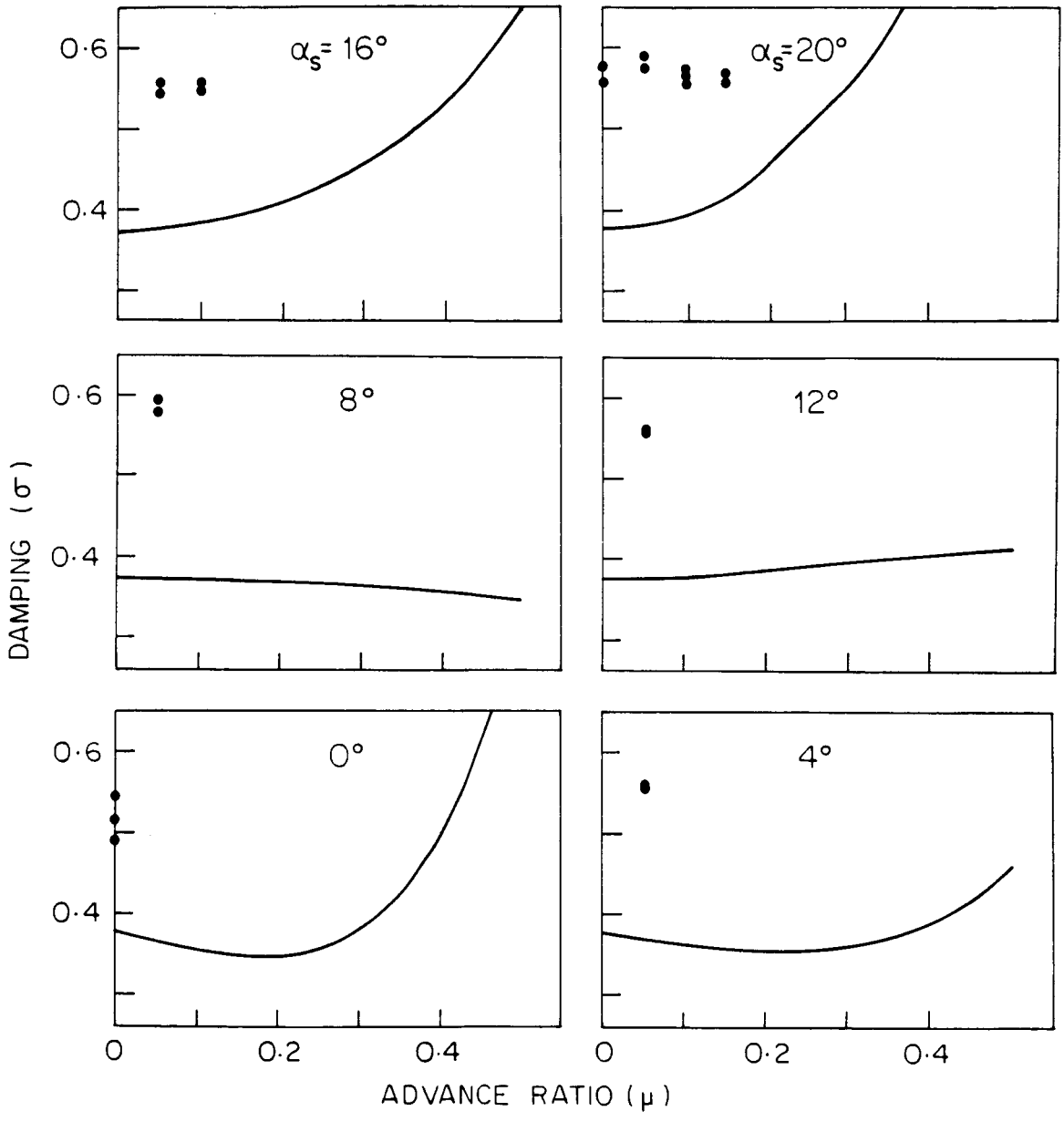

FIG. 10 LAG REGRESSING MODE DAMPING $\theta_0 = 6°$, $\Omega = 1000$, $R = 1$
(THEORETICAL ——, EXPERIMENTAL ••)

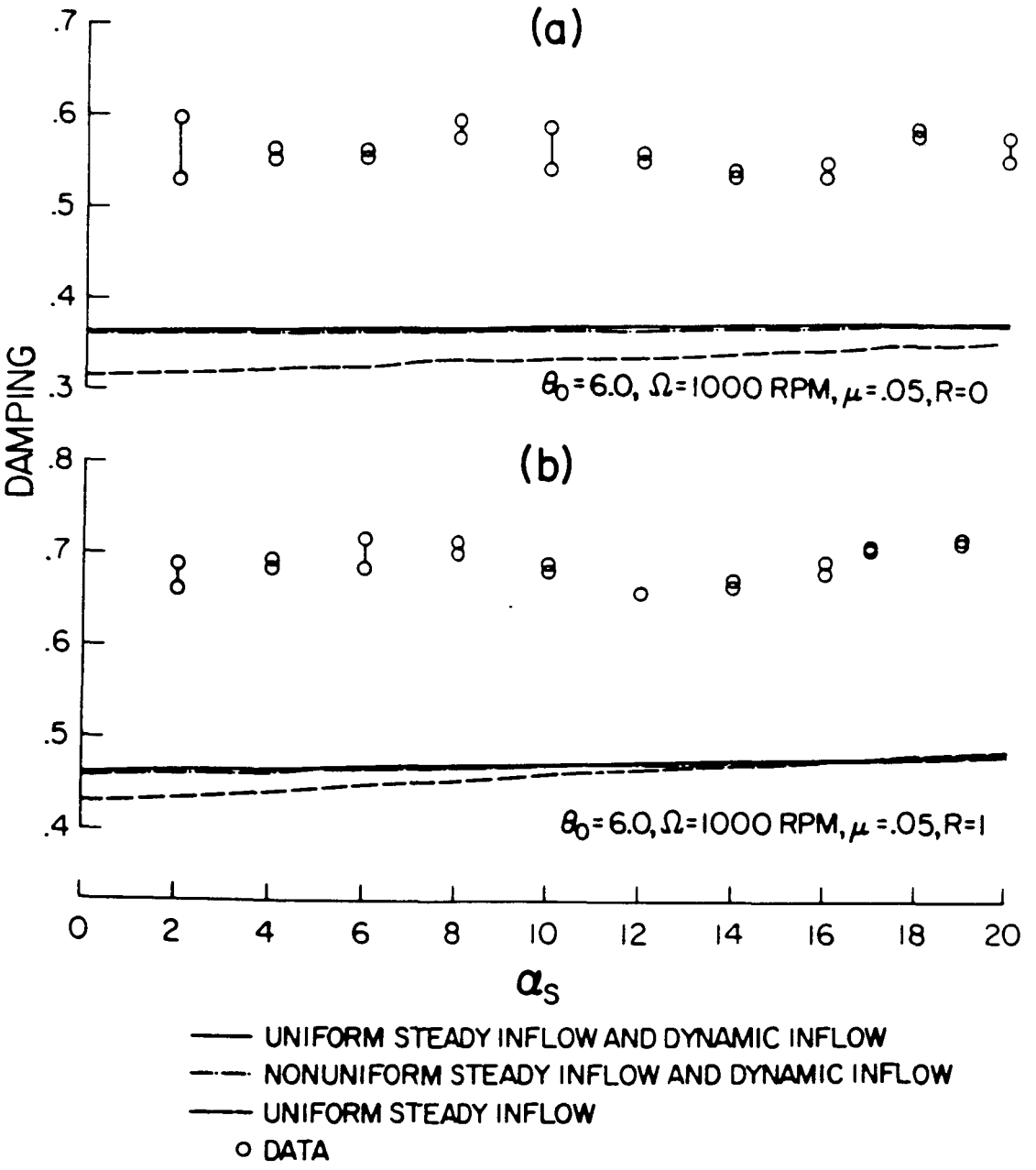

Fig. 11 LAG REGRESSING MODE DAMPING

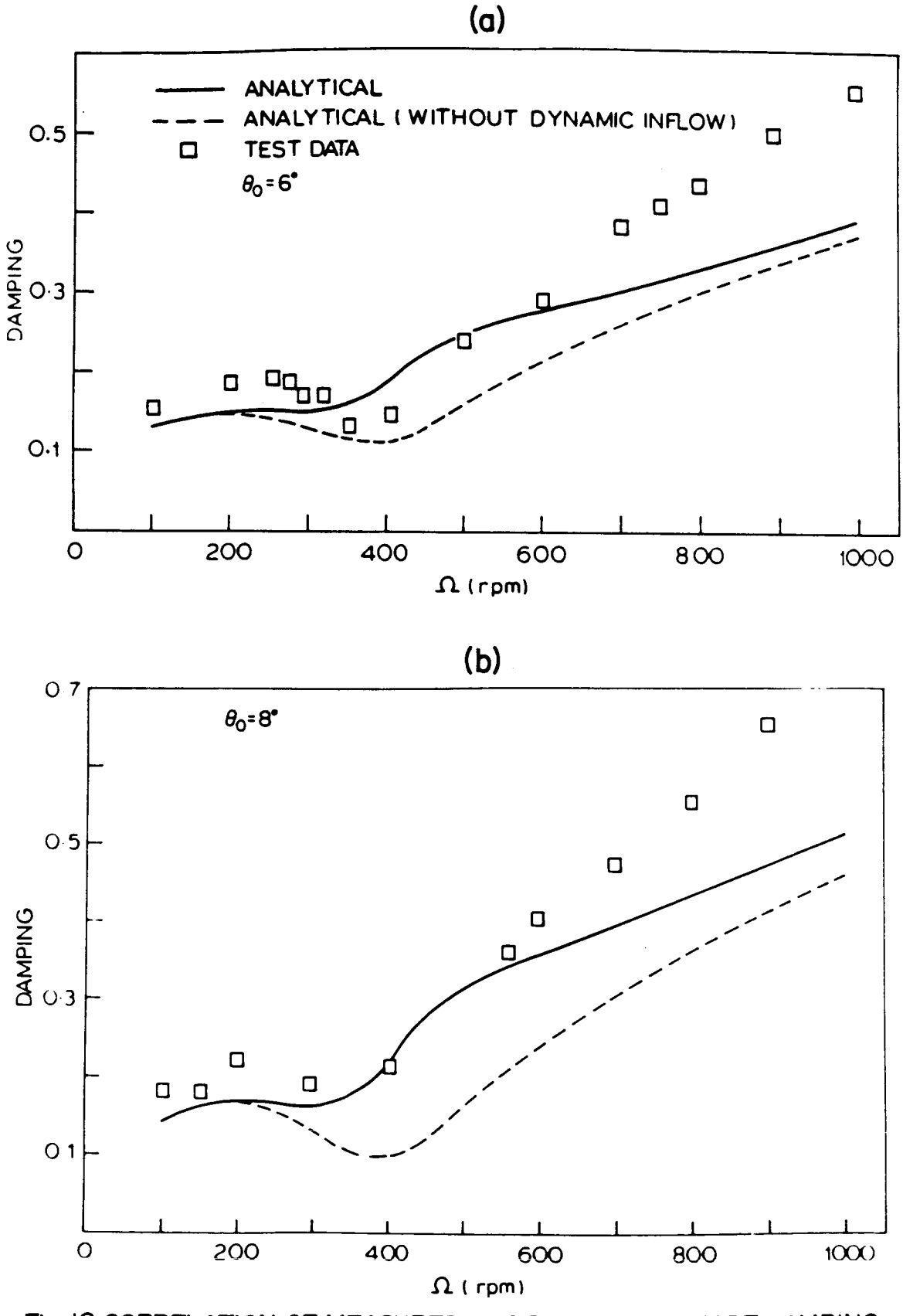

Fig.12 CORRELATION OF MEASURED LAG REGRESSING MODE DAMPING WITH PREDICTED VALUES IN HOVER

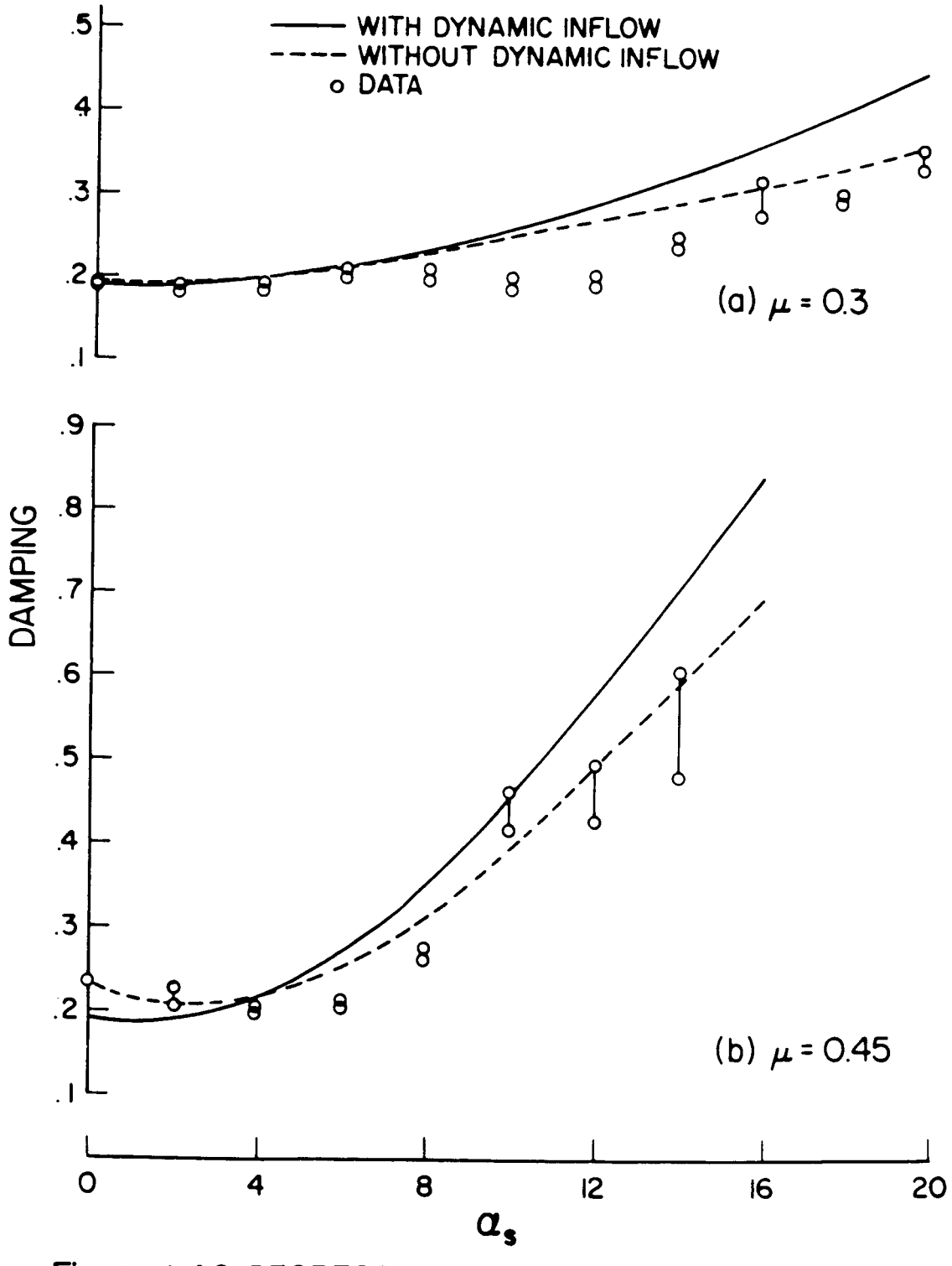

Fig.13 LAG REGRESSING MODE DAMPING CORRELATIONS, IN SUBSTALL AND STALL (Ω=1000 RPM, R=0, θ_o= 0°)